Progress In Electromagnetics Research, PIER 97, 275–290, 2009

A DATA-ADAPTIVE PROBABILITY-BASED FAST ERT INVERSION METHOD

P. Mauriello

Department of Science and Technology for Environment and Territory
University of Molise
Campobasso, Italy

D. Patella

Department of Physical Sciences
University Federico II
Naples, Italy

Abstract—An easy and fast Probability-based Electrical Resistivity Tomography Inversion (PERTI) algorithm is proposed. The simplest theory follows from the principles of the probability tomography imaging, previously developed for the ERT method of geophysical prospecting. The new inversion procedure is based on a formula which provides the resistivity at any point of the surveyed volume as a weighted average of the apparent resistivity data. The weights are obtained as the Frechet derivatives of the apparent resistivity function of a homogeneous half-space, where a resistivity perturbation is produced in an arbitrary small cell of the discretised surveyed volume. Some 2D and 3D synthetic examples are presented, for which the results of the PERTI method are compared with the inverted models derived from the application of the commercial inversion softwares ERTLAB by Multi-Phase Technologies and Geostudi Astier, and RES2DINV and RES3DINV by Geotomo Software. The comparison shows that the new approach is generally as efficacious as the previous methods in detecting, distinguishing and shaping the sources of the apparent resistivity anomalies. Less certain appears, however, its ability to approach the true resistivity of the source bodies. Main peculiarities of the new method are: (i) unnecessity of a priori information and hence full and unconstrained data-adaptability; (ii) decrease of computing time, even two orders of magnitude shorter than that required by commercial softwares in complex 3D cases using the

Corresponding author: D. Patella (patella@na.infn.it).

same PC; (iii) real-time inversion directly in the field, thus allowing for fast modifications of the survey plan to better focus the expected targets; (iv) total independence from data acquisition techniques and spatial regularity, (v) possibility to be used as an optimum starting model in standard iterative inversion processes in order to speed up convergence.

1. INTRODUCTION

Probability tomography is a 3D imaging approach useful to explore the information content of a geophysical field dataset. The theory was originally developed for the self-potential method [1] and then extended to the resistivity method to image the most probable position and shape of the source bodies responsible of the apparent resistivity anomalies [2–5].

Although able to spatially distinguish resistivity highs and lows with respect to a reference background resistivity, the probability tomography was formulated in such a way to preclude the direct possibility to provide an estimate of the intrinsic resistivities of the target bodies. In near-surface geoelectrics, this aspect has only rarely been considered a serious shortage, as the determination of the resistivity of the source bodies in many target-oriented applications is not so important as the knowledge of their position and shape. Many datasets have been successfully interpreted on this semi-quantitative basis, e.g., in archaeological prospection [6, 7]. In all the cases in which the correct estimate of the true resistivity has been considered essential for assessing the inner properties of the target, the probability tomography has been used as a means able to provide robust and confident geometrical constraints in any of the standard inversion routines [8].

In order to overcome such a limitation, we propose in this paper a new fast inversion method, which is directly deduced from the principles of the probability tomography. In the following sections, at first we recall these principles, from which we then derive the solution to the inversion problem. In order to elicit the main features of the new probability-based electric resistivity tomography inversion method, from now onward PERTI, some synthetic examples are analysed and the PERTI results are compared with those obtained by the commercial softwares ERTLAB by Multi-Phase Technologies (www.mpt3d.com) and Geostudi Astier (www.geoastier.com), and RES2D/3DINV by Geotomo Software (www.geoelectrical.com), based on Loke and Barker's original approach [9].

2. OUTLINE OF THE PROBABILITY TOMOGRAPHY

This section deals with the main aspects of the geoelectrical probability tomography, fully depicted in previous articles [2–5]. In the original formulation of the geoelectrical probability tomography [2], the volume V below the flat ground surface where a geoelectric survey is carried out was assumed to be composed of M cells with a small volume ΔV, each identified by its intrinsic resistivity, ρ_m, and centred at (x_m, y_m, z_m) $(m = 1, \ldots, M)$. Accordingly, the nth apparent resistivity, $\rho_{a,n}$ $(n = 1, \ldots, N)$, was expanded in Taylor series stopped to the first derivative term, as

$$\Delta\rho_{a,n} = \rho_{a,n} - \rho_{a,n}^{ref} \approx \sum_{m=1}^{M} (\partial\rho_{a,n}^{ref} \Big/ \partial\rho_m)\Delta\rho_m. \tag{1}$$

In Eq. (1), $\Delta\rho_{a,n}$ is the difference between $\rho_{a,n}$ and an apparent resistivity, $\rho_{a,n}^{ref}$, derived from a reference model using the same location of the four-electrode array as for $\rho_{a,n}$, and $\Delta\rho_m$ is the departure of ρ_m from the resistivity, ρ_m^{ref}, assigned by the reference model to the mth cell.

Then, the information power Λ associated with the modified dataset $\Delta\rho_{a,n}$ was introduced as

$$\Lambda = \sum_{n=1}^{N} (\Delta\rho_{a,n})^2, \tag{2}$$

which, using Eq. (1), was rewritten as

$$\Lambda = \sum_{m=1}^{M} \Delta\rho_m \sum_{n=1}^{N} \Delta\rho_{a,n}(\partial\rho_{a,n}^{ref} \Big/ \partial\rho_m). \tag{3}$$

Finally, the application of Schwarz's inequality to any mth element of the first sum, i.e.,

$$\left[\sum_{n=1}^{N} \Delta\rho_{a,n}(\partial\rho_{a,n}^{ref} \Big/ \partial\rho_m)\right]^2 \leq \sum_{n=1}^{N} \Delta\rho_{a,n}^2 \sum_{n=1}^{N} (\partial\rho_{a,n}^{ref} \Big/ \partial\rho_m)^2, \tag{4}$$

allowed the source cell occurrence probability function, $\eta_m[\equiv \eta(x_m, y_m, z_m)]$, to be introduced as

$$\eta_m = C_m \sum_{n=1}^{N} \Delta\rho_{a,n}(\partial\rho_{a,n}^{ref} \Big/ \partial\rho_m), \tag{5}$$

where

$$C_m = \left[\sum_{n=1}^{N} (\Delta\rho_{a,n})^2 \sum_{n=1}^{N} (\partial\rho_{a,n}^{ref} \Big/ \partial\rho_m)^2 \right]^{-1/2} . \tag{6}$$

The η_m-function, with $\eta_m \in [-1, +1]$, was assumed to provide a measure of the probability with which a source pole, responsible of the $\rho_{a,n}$ dataset, is present in the mth cell. The role of probability attributed to η_m was motivated as follows, noting that a probability measure Ψ is defined as a function assigning to every subset E of a space of states U a real number $\Psi(E)$ such that [10]

$$\Psi(E) \geq 0, \text{for every } E, \tag{7a}$$

$$\text{if } E \cap F \equiv 0, \text{with } E, F \subset U, \Psi(E \cup F) = \Psi(E) + \Psi(F), \tag{7b}$$

$$\Psi(U) = 1. \tag{7c}$$

Considering that the presence of a source pole in V is independent from the presence of other poles at other points of V, the function

$$\Psi_m = |\eta_m| \Big/ \int_V |\eta_m| \, dV \tag{8}$$

has the meaning of a probability density, since it allows a measure of the probability to find a source pole in the mth cell to be determined in agreement with the axioms (7a)–(7c). Practically, η_m differs from Ψ_m only for an unknown factor and has also the advantage to give the sign of the source pole. Thus, by convention η_m was assumed as a probability measure for a source pole to occur in the mth cell.

The 3D probability tomography was conceived as a scanning tool driven by the Frechet derivative $\partial\rho_{a,n}^{ref} \Big/ \partial\rho_m$, whose expression depends on the reference model and the position of the four-electrode array [11]. Using Eq. (5), a positive η_m at a point (x_m, y_m, z_m) was therefore assumed to give the occurrence probability of a positive source pole, i.e., the non vanishing probability to find, in the cell centred at that point, an increase of resistivity with respect to the reference resistivity ρ_m ($\Delta\rho_m > 0$). Conversely, a negative η_m was assumed to give the occurrence probability of a negative source pole, i.e., the non vanishing probability to find a decrease of resistivity with respect to the reference resistivity ρ_m ($\Delta\rho_m < 0$). Finally, a null value of η_m was assumed to represent the situation in which no anomaly source pole occurs in the cell centred at (x_m, y_m, z_m), i.e., the intrinsic resistivity in the cell does not differ from the reference resistivity ($\Delta\rho_m = 0$).

To easily derive the formula of the Frechet derivative $\partial\rho_{a,n}^{ref} \Big/ \partial\rho_m$ and to construct the modified dataset $\Delta\rho_{a,n}$, a simple homogeneous

half-space was suggested as reference model, by taking as uniform resistivity the average apparent resistivity or any other value assumed to be compatible with the expected background resistivity. The relative meaning of the probability tomography imaging, due to this rather arbitrary choice of the reference resistivity, was amply dealt with by Mauriello and Patella [2].

3. THE PROBABILITY-BASED ERT INVERSION

The starting assumption for the PERTI method is that the reference uniform resistivity is no longer pre-assigned but assumed to be the unknown value ρ_m that corresponds to a generic mth cell centred at (x_m, y_m, z_m). Such an assumption allows η_m to be rewritten as

$$\eta_m = C_m \sum_{n=1}^{N} (\rho_{a,n} - \rho_m)(\partial \rho_{a,n}^{ref} \Big/ \partial \rho_m). \tag{9}$$

The rationale for the new inversion tool is that if at a point (x_m, y_m, z_m) it results $\eta_m = 0$, then in the cell centred at (x_m, y_m, z_m) the probability to find an increase or a decrease of the resistivity with respect to ρ_m is zero. In other words, in that cell the intrinsic resistivity does not differ from ρ_m. Thus, referring to Eq. (5), since C_m is always different from zero, the $\eta_m = 0$ condition leads to

$$\rho_m = \sum_{n=1}^{N} \rho_{a,n}(\partial \rho_{a,n}^{ref} \Big/ \partial \rho_m) \Bigg/ \sum_{n=1}^{N} (\partial \rho_{a,n}^{ref} \Big/ \partial \rho_m), \tag{10}$$

which represents the required solution for the application of the PERTI method. We only need to change repeatedly the coordinates (x_m, y_m, z_m) to retrieve, point by point, the resistivity pattern within V.

The certainty hypothesis, upon which the derivation of Eq. (10) has been based, must, of course, be intended within the limits imposed by the data sampling rate and accuracy, the survey extent and, mostly, the Born approximation used for the initial definition of $\Delta\rho_{a,n}$ given in Eq. (1).

In conclusion, by this very simple and rapid approach, the intrinsic resistivity at a point of the surveyed volume is nothing but a weighted average of the apparent resistivity values, using the Frechet derivatives as weights depending on the coordinates of the given point.

4. ADAPTATION TO THE DIPOLE-DIPOLE ARRAY

This section deals with the main aspects of the well known dipole-dipole configuration for the acquisition of geoelectrical data. In near-

surface surveys, the dipole-dipole (DD) (Fig. 1) is the most convenient four-electrode device, since it provides a very detailed lateral bounding of vertical features. The DD device is normally used in profiling mode to map lateral as well as depth variations of the resistivity. The convention for the DD device illustrated in Fig. 1 is that current and voltage dipole lengths are the same, a, and the spacing between the dipoles is an integer multiple k of a.

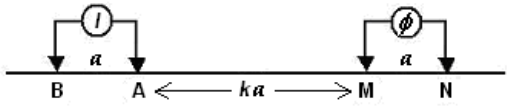

Figure 1. The dipole-dipole array. A, B and M, N are the current (I) and potential (ϕ) dipole, respectively. The dipole length is a and k determines the dipolar spacing as an integer multiple of a.

The ERT approach consists in taking determinations of $\rho_{a,n}$ at as many locations as possible and involves the joint inversion of the many independent tests. The inversion of a $\{\rho_{a,n}\}$ dataset, collected by the described DD profiling field technique, gives rise to a 2D ERT model. If one assembles a set of p parallel DD profiles, the common inversion of the multiple $\{\rho_{a,n}\}$ dataset provides a 3D ERT model.

The DD apparent resistivity is calculated using the formula $\rho_{a,n} = (K/I_n)\Delta\phi_n$, where:

- I_n is the intensity of the primary current injected into the ground through the electrodes A and B in the nth position ($n = 1, 2, \ldots, N$), say A_n and B_n,
- $K = \pi ak(k{+}1)(k{+}2)$ is the DD geometrical factor, where a is the spread of the dipoles and k the sampling step running index along the profile axis, taken parallel to the x-axis of a reference system with the (x, y)-plane coinciding with the ground surface, assumed locally flat, and the z-axis positive downwards, and
- $\Delta\phi_n$ is the potential difference across the electrodes M and N in the nth position, say M_n and N_n, expanded as $\Delta\phi_n = \phi^{\mathrm{A}_n}_{\mathrm{M}_n} - \phi^{\mathrm{B}_n}_{\mathrm{M}_n} - \phi^{\mathrm{A}_n}_{\mathrm{N}_n} + \phi^{\mathrm{B}_n}_{\mathrm{N}_n}$.

The Frechet derivative of $\rho^{ref}_{a,n}$, is thus made explicit as

$$\frac{\partial \rho^{ref}_{a,n}}{\partial \rho_m} = \frac{K}{I_n}\frac{\partial}{\partial \rho_m}\left(\phi^{\mathrm{A}_n}_{\mathrm{M}_n} - \phi^{\mathrm{B}_n}_{\mathrm{M}_n} - \phi^{\mathrm{A}_n}_{\mathrm{N}_n} + \phi^{\mathrm{B}_n}_{\mathrm{N}_n}\right). \tag{11}$$

If the reference model is a homogeneous half space, indicating with y_p the coordinate along the y-axis of the pth DD profile, the four

Frechet derivatives of the potential function are [2]

$$\frac{\partial \phi_{\mathrm{M}_n}^{\mathrm{A}_n}}{\partial \rho_m} = \frac{I_n \Delta V}{4\pi^2} \cdot \frac{\Delta x_1 \Delta x_2 + \Delta r^2}{\left(\Delta x_1^2 + \Delta r^2\right)^{3/2} \left(\Delta x_2^2 + \Delta r^2\right)^{3/2}}, \tag{12a}$$

$$\frac{\partial \phi_{\mathrm{M}_n}^{\mathrm{B}_n}}{\partial \rho_m} = \frac{I_n \Delta V}{4\pi^2} \cdot \frac{\Delta x_3 \Delta x_2 + \Delta r^2}{\left(\Delta x_3^2 + \Delta r^2\right)^{3/2} \left(\Delta x_2^2 + \Delta r^2\right)^{3/2}}, \tag{12b}$$

$$\frac{\partial \phi_{\mathrm{N}_n}^{\mathrm{A}_n}}{\partial \rho_m} = \frac{I_n \Delta V}{4\pi^2} \cdot \frac{\Delta x_1 \Delta x_4 + \Delta r^2}{\left(\Delta x_1^2 + \Delta r^2\right)^{3/2} \left(\Delta x_4^2 + \Delta r^2\right)^{3/2}}, \tag{12c}$$

$$\frac{\partial \phi_{\mathrm{N}_n}^{\mathrm{B}_n}}{\partial \rho_m} = \frac{I_n \Delta V}{4\pi^2} \cdot \frac{\Delta x_3 \Delta x_4 + \Delta r^2}{\left(\Delta x_3^2 + \Delta r^2\right)^{3/2} \left(\Delta x_4^2 + \Delta r^2\right)^{3/2}}, \tag{12d}$$

where it is

$$\Delta x_1 = x_m - x_{\mathrm{A}_n}, \tag{13a}$$

$$\Delta x_2 = x_m - x_{\mathrm{M}_n}, \tag{13b}$$

$$\Delta x_3 = x_m - x_{\mathrm{B}_n}, \tag{13c}$$

$$\Delta x_4 = x_m - x_{\mathrm{N}_n}, \tag{13d}$$

$$\Delta r^2 = (y_m - y_p)^2 + z_m^2. \tag{13e}$$

5. SYNTHETIC TESTS

In order to evaluate the performance of the PERTI method and to be more specific on how the technique is used, we study some synthetic examples of 2D and 3D structures. The results from the application of Eq. (10) will be compared with those coming from the use of the ERTLAB and RES2DINV or RES3DINV softwares. The 2D synthetic cases have been extracted from the Geotomo Software inversion manual.

5.1. The 2D Three-prism Model

A 2D model is considered as depicted in Fig. 2(a). Three infinitely long horizontal prisms with rectangular cross-section and resistivity 500, 10 and 30 Ωm, respectively, are placed inside a uniform half-space with resistivity 100 Ωm. The structure is assumed to be prospected by a DD array with spacing of 1 m along a profile of 36 m perpendicular to the 2D strike. The three prisms are 3 m wide and 1.3 m high, with the top surfaces placed at 1.5 m of depth. The $\{\rho_{a,n}\}$ pseudosection, contaminated by a 5% random noise, is plotted in Fig. 2(b).

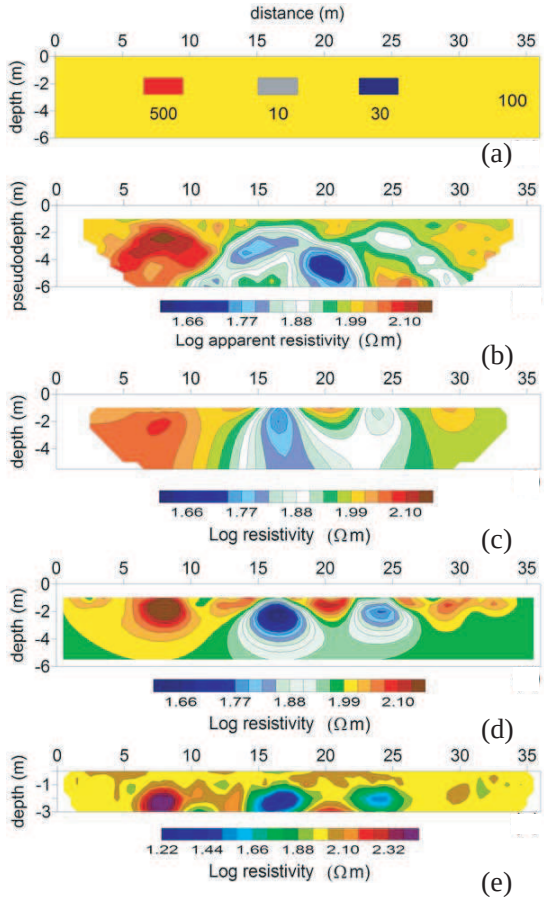

Figure 2. A comparative analysis of the PERTI, ERTLAB and RES2DINV approaches applied to the 2D three-prism model. (a) The simulated pseudosection, (b) and the model reconstruction by the PERTI, (c) ERTLAB, (d) and RES2DINV, (e) algorithms.

Figures 2(c)–(e) show the resistivity sections obtained by the PERTI, ERTLAB and RES2DINV softwares. The ERTLAB and RES2DINV sections are better representative of the presence of the prisms, although the algorithms show the tendency to generate artefacts either in the top part, viz. ERTLAB, or in the bottom part, viz. RES2DINV, likely due to noise. On the contrary, the PERTI algorithm provides a smoother section with the tendency to weaken not only the resistivity contrasts, but, significantly, also the artefacts due to noise. However, it must be pointed out that the RES2DINV

Table 1. A comparative analysis of the PERTI, ERTLAB and RES2DINV approaches applied to the 2D three-prism model shown in Fig. 2(a). The estimated resistivity range in correspondence of the three blocks.

	Prism (500 Ωm)	**Prism (10 Ωm)**	**Prism (30 Ωm)**
PERTI	118–134 Ωm	52–59 Ωm	67–76 Ωm
ERTLAB	162–209 Ωm	52–59 Ωm	55–71 Ωm
RES2DINV	247–293 Ωm	23–33 Ωm	33–64 Ωm

section, differently from the ERTLAB and mostly the PERTI section, displays a significant deepening of the centres of the first two blocks from left, which appear to be located at around 2.5 m of depth, instead of 2.15 m.

As it concerns the resistivity of the prisms, considering the portion of the nuclei nearly located in the area occupied by them, the estimates listed in Table 1 have been obtained. It must be pointed out that the RES2DINV software does not allow for an inversion below 3 m of depth. However, in this case, the RES2DINV algorithm seems the one that best approaches the true resistivities of the prisms and allows for a clearer distinction between the prisms and the background, followed by the ERTLAB algorithm.

5.2. The Fault and Prism Model

A 2D model is again considered as in Fig. 3(a). A faulted structure with resistivity 100 Ωm is placed in horizontal and vertical contact with a 10 Ωm material. In this conductive material, an infinitely long horizontal prism, 5 m wide, 2.4 m high and with resistivity 2 Ωm, is placed. Both structures have the top surface at 0.8 m of depth. A DD survey with a spacing of 1 m is simulated along a straight profile of 60 m perpendicular to the 2D strike. The $\{\rho_{a,n}\}$ pseudosection, contaminated again by a 5% random noise, is plotted in Fig. 3(b).

Figures 3(c)–(e) show the resistivity sections obtained by the PERTI, ERTLAB and RES2DINV softwares. It is evident that the best geometrical resolution is now provided by the PERTI and RES2DINV tools. In fact, both inversion methods give a model section reasonably conforming to the original section, whereas the ERTLAB algorithm does not respond satisfactorily as to the definition of the faulted structure. It can finally be noted the tendency of the RES2DINV approach to raise the bottom of the conductive block a little above the

true depth.

As it concerns the resistivity of the faulted layer and the prism, considering again the portion of the nuclei nearly located in the area occupied by them, the estimates listed in Table 2 have been obtained. Once again, the RES2DINV software has not allowed the inversion to be run below 3 m of depth. In this case the PERTI algorithm appears to be the one that best approaches the true section.

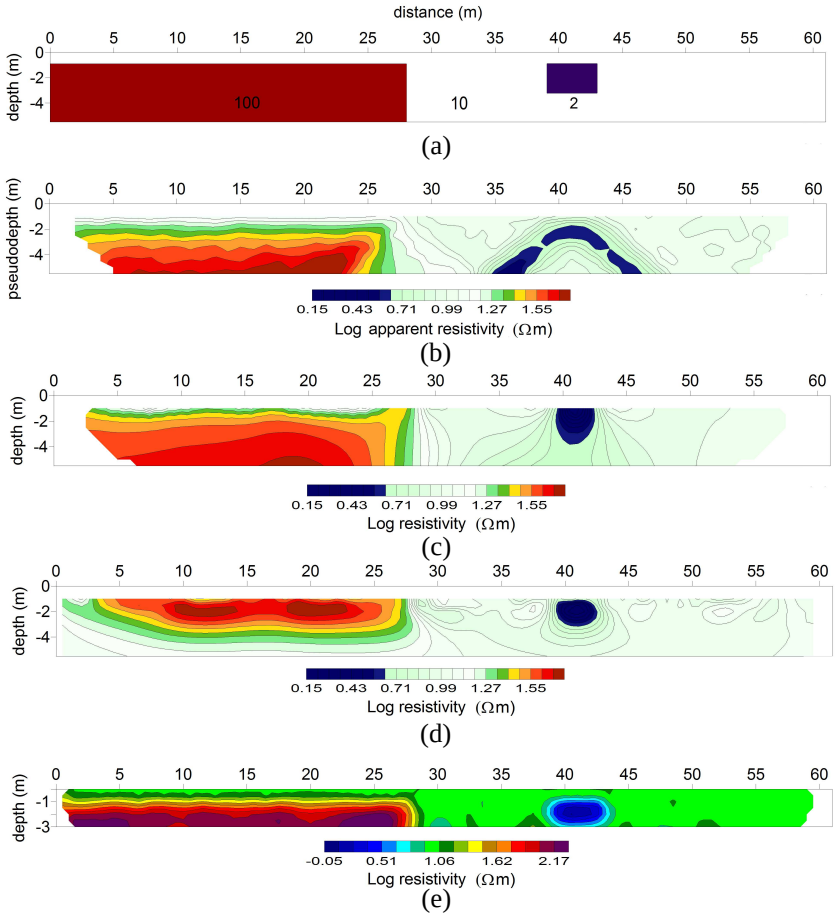

Figure 3. A comparative analysis of the PERTI, ERTLAB and RES2DINV approaches applied to the 2D fault and prism model. (a) The simulated pseudosection, (b) and the model reconstruction by the PERTI, (c) ERTLAB, (d) and RES2DINV, (e) algorithms.

Table 2. A comparative analysis of the PERTI, ERTLAB and RES2DINV approaches applied to the 2D fault and prism model shown in Fig. 3(a). The estimated resistivity range in correspondence of the faulted layer and prism.

	Faulted layer (100 Ωm)	**Prism (2 Ωm)**
PERTI	19–58 Ωm	1.4–4.4 Ωm
ERTLAB	19–58 Ωm	1.4–4.4 Ωm
RES2DINV	22–219 Ωm	1.5–6.2 Ωm

5.3. The Two-layer and Dyke Model

The last 2D model which has been dealt with is drawn in Fig. 4(a). A two-layer structure is considered where the first 20 m thick overburden with resistivity of 300 Ωm overlies a resistive substratum with resistivity of 1000 Ωm. A vertical dyke, only 5 m wide and with resistivity 10 Ωm, is placed inside the substratum. A DD survey with a spacing of 5 m is simulated along a profile of 295 m perpendicular to the strike direction. The $\{\rho_{a,n}\}$ pseudosection, corrupted again by a 5% random noise, is plotted in Fig. 4(b).

Figures 4(c)–(e) show the model sections obtained by the PERTI, ERTLAB and RES2DINV methods. The PERTI algorithm provides a geometrical solution that appears to conform to the true section, although with an exceedingly large dyke breadth, which is, however, very similar to that appearing in the ERTLAB and RES2DINV modelled sections. These two last approaches show the tendency to image the two portions of the substratum, on both sides of the dyke, as two laterally confined blocks, differently from the PERTI inversion software, which provides, instead, a better image of the two-layer sequence.

As it concerns the resistivity of the two-layer and the dyke, considering again the portion of the nuclei nearly located in the area occupied by them, the estimates listed in Table 3 have been obtained.

5.4. The Archaeological Masonry Model

To conclude this section, we study now the responses from the 3D model in Fig. 5(a). The model aims at simulating a buried archaeological structure consisting of a sequence of walls disposed at right angle, bounding two adjacent rooms, each with its own entrance.

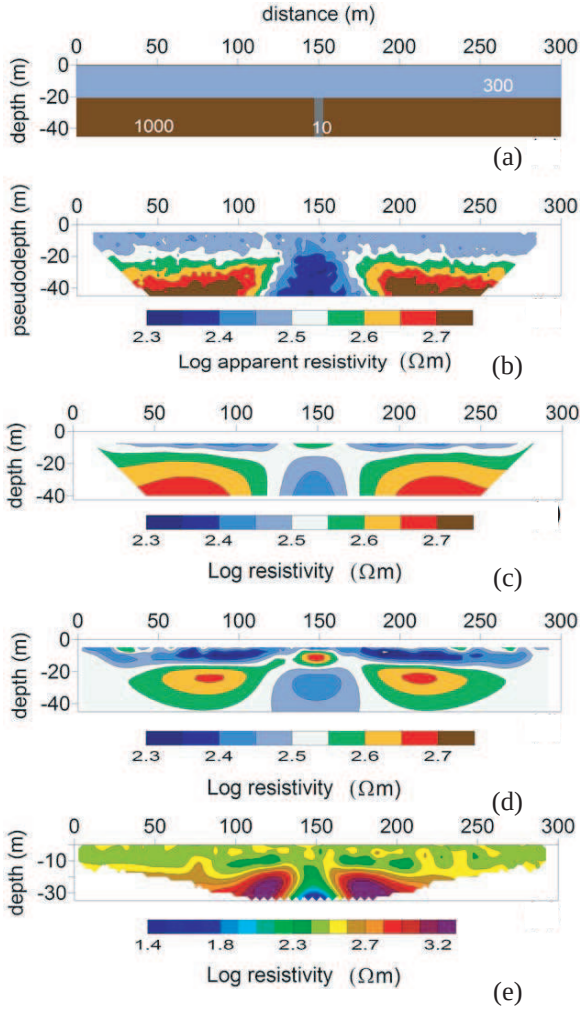

Figure 4. A comparative analysis of the PERTI, ERTLAB and RES2DINV approaches applied to the 2D two-layer and dyke model. (a) The pseudosection, (b) and the model reconstruction by the PERTI, (c) ERTLAB, (d) and RES2DINV, (e) algorithms.

The masonry structure is placed between 0.7 and 1.6 m of depth and is given the resistivity of 150 Ωm, in contrast with the 50 Ωm of the hosting half-space. A DD survey with a 1 m dipole length is simulated along a set of profiles parallel to the x-axis and spaced 1 m apart, up to the pseudodepth index $k = 10$.

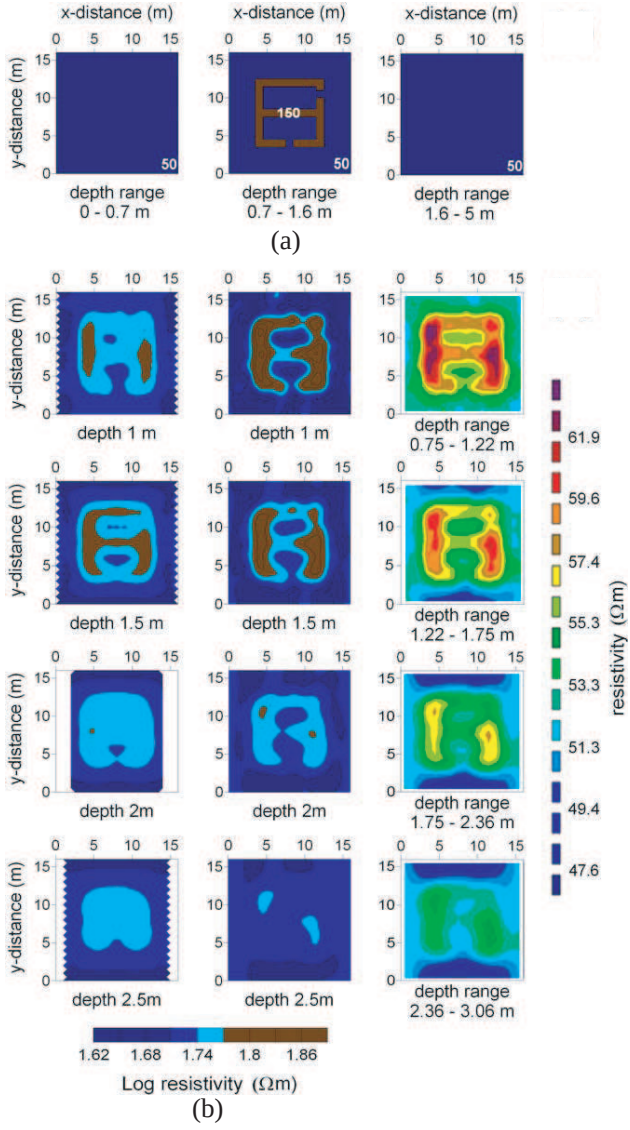

Figure 5. A comparative analysis of the PERTI, ERTLAB and RES3DINV approaches applied to a 3D archaeological masonry model. (a) Inverted model horizontal slice sequence at the depths of 1 m, 1.5 m, 2 m, and 2.5 m, (b) using the PERTI (left column), ERTLAB (mid column) and RES3DINV (right column) algorithms.

Table 3. A comparative analysis of the PERTI, ERTLAB and RES2DINV approaches applied to the 2D two-layer and dyke model shown in Fig. 4(a). The estimated resistivity range in correspondence of the two-layer and dyke.

	Top layer (300 Ωm)	**Substratum (1000 Ωm)**	**Dyke (10 Ωm)**
PERTI	251–398 Ωm	447–551 Ωm	251–282 Ωm
ERTLAB	211–501 Ωm	447–551 Ωm	251–282 Ωm
RES2DINV	200–501 Ωm	501–2113 Ωm	33–200 Ωm

Figure 5(b) displays the inverted horizontal slices at four different depths every 0.5 m from 1 m down to 2.5 m, as resulting from the PERTI (left column), ERTLAB (mid column) and RES3DINV (right column) approaches. All of the three algorithms provide a correct lateral definition of the masonry structure. However, the PERTI and ERTLAB methods appear to provide the best depth collocation of the masonry structure, conforming to the initial model, whereas the RES3DINV software shows some difficulty to close the bottom of the walls at the proper depth. As to the entrances to the two rooms, the PERTI algorithm appears to be the one that provides the correct positioning of both entrances. As it concerns the resistivity of the masonry structure and hosting rock, the PERTI and ERTLAB inversions have given values in the range 59–78 Ωm and 42–55 Ωm, respectively, while the RES3DINV in the range 59–64 Ωm and 49–56 Ωm, respectively.

In 3D cases, which involve datasets much heavier than in 2D cases, computing time becomes the main criterion for the selection among inversion methods with comparable resolution. In the case of Fig. 5, the time required by the PERTI algorithm using a standard PC was only about 3 min, by far shorter than the time required by the ERTLAB software (more than 250 min) and the RES3DINV demo version (about 30 min).

6. CONCLUSION

We have proposed an easy and fast 3D electrical resistivity inversion algorithm, which has been deduced from the 3D probability tomography imaging theory, shown in previous papers. The new inversion procedure is based on a formula, which provides the resistivity at any point of the surveyed volume as a weighted average of the apparent resistivity dataset. The weights have been expressed as the

Frechet derivatives of the apparent resistivity for a homogeneous half-space, where a resistivity perturbation is produced in an arbitrary small cell of the discretised survey volume. The results of the new inversion method applied to some 2D and 3D synthetic cases have been compared with those obtained from the application of the ERTLAB and RES2DINV or RES3DINV softwares. The comparison has shown that the new approach is generally as efficacious as the two older tools in detecting, distinguishing and shaping the sources of the observed apparent resistivity anomalies. The estimate of the intrinsic resistivity of the source bodies, has appeared closely comparable with that of the ERTLAB software, but sensibly less precise than that of the RES2DINV approach.

Main features of the PERTI method are: (i) unnecessity of a priori information; (ii) full, unconstrained adaptability to any kind of dataset, including the case of non-flat topography; (ii) drastic reduction of computing time of even two orders of magnitude, with respect to the previous methods in complex 3D cases using the same PC; (iii) real-time inversion directly in the field, thus allowing for fast modifications of the survey plan to better focus the expected targets; (iv) full independence from data acquisition techniques and spatial regularity, (v) possibility to be used as an optimum starting model in standard iterative inversion processes in order to speed up convergence.

REFERENCES

1. Patella, D., "Introduction to ground surface self-potential tomography," *Geophys. Prosp.*, Vol. 45, 653–681, 1997.
2. Mauriello, P. and D. Patella, "Resistivity anomaly imaging by probability tomography," *Geophys. Prosp.*, Vol. 47, 411–429, 1999.
3. Mauriello, P. and D. Patella, "Resistivity tensor probability tomography," *Progress In Electromagnetics Research B*, Vol. 8, 129–146, 2008.
4. Mauriello, P. and D. Patella, "Geoelectrical anomalies imaged by polar and dipolar probability tomography," *Progress In Electromagnetics Research*, PIER 87, 63–88, 2008.
5. Alaia, R., D. Patella, and P. Mauriello, "Application of geoelectrical 3D probability tomography in a test-site of the archaeological park of Pompei (Naples, Italy)," *J. Geophys. Eng.*, Vol. 5, 67–76, 2008.
6. Alaia, R., D. Patella, and P. Mauriello, "Imaging multipole self-potential sources by 3D probability tomography," *Progress In Electromagnetics Research B*, Vol. 14, 311–339, 2009.

7. Compare, V., M. Cozzolino, P. Mauriello, and D. Patella, "Three-dimensional resistivity probability tomography at the prehistoric site of Grotta Reali (Molise, Italy)," *Archaeol. Prosp.*, Vol. 16, 53–63, 2009.
8. Zhou, B. and S. A. Greenhalgh, "Rapid 2D/3D crosshole resistivity imaging using the analytic sensitivity function," *Geophysics*, Vol. 67, 755–765, 2002.
9. Loke, M. H. and R. D. Barker, "Rapid least-squares inversion of apparent resistivity pseudosections by a quasi-Newton method," *Geophys. Prosp.*, Vol. 44, 131–152, 1996.
10. Gnedenko, B. V., *Kurs Teorii Verojatnostej*, Mir, Moscow, 1979.
11. Barker, R. D., "A simple algorithm for electrical imaging of the subsurface," *First Break*, Vol. 10, 53–62, 1992.